Analysis of Surface Enhancement by a Porous Substrate

Kambiz Vafai

Sung-Jin Kim

Department of Mechanical Engineering,
The Ohio State University,
Columbus, OH 43210

Convective flow and heat transfer through a composite porous/fluid system have been studied numerically. The composite medium consists of a fluid layer overlaying a porous substrate, which is attached to the surface of the plate. The numerical simulations focus primarily on flows that have the boundary layer characteristics. However, the boundary layer approximation was not used. A general flow model that accounts for the effects of the impermeable boundary and inertia is used to describe the flow inside the porous region. Several important characteristics of the flow and temperature fields in the composite layer are reported. The dependence of these characteristics on the governing parameters such as the Darcy number, the inertia parameter, the Prandtl number, and the ratio of the conductivity of the porous material to that of the fluid is also documented. The results of this investigation point out a number of interesting practical applications such as in frictional drag reduction, and heat transfer retardation or enhancement of an external boundary.

1 Introduction

The problem of convective heat transfer and fluid flow over a horizontal flat plate has received considerable attention since the early work of Blasius. The analogous problem in fluid-saturated porous media has also drawn much attention due to such diverse applications as drying processes, thermal insulation, direct contact heat exchangers, heat pipe, filtration, etc. These applications made it imperative that a deeper insight into porous media transport processes must be gained. While numerous studies have been performed in the above areas, little attention has been focused on the problem in which a porous/fluid composite system is involved. This type of composite system is encountered in various applications such as solidification of castings, crude oil extraction, thermal insulation, geophysical systems, etc.

Of the few investigations in the porous/fluid composite systems, Poulikakos's (1986) work can be cited. Poulikakos (1986) studied the buoyancy-driven flow instability numerically for a fluid layer extending over a porous substrate in a cavity heated from the bottom. Beckermann et al. (1987, 1988) and Sathe et al. (1988) performed numerical and experimental investigations on the natural convection heat transfer and fluid flow in a vertical rectangular enclosure that is partially filled with a fluid-saturated porous medium. They found that the amount of fluid penetrating from the fluid region into the porous region depends strongly on the Darcy and Rayleigh numbers. More relevant to the present study is the work of Vafai and Thiyagaraja (1987). They analytically investigated the fully developed forced convection for the interface region between a fluid layer and a porous medium. Another related problem is that of Poulikakos and Kazmierczak (1987), in which a fully developed forced convection in a channel that is partially filled with a porous matrix was investigated. They showed the existence of a critical thickness of the porous layer at which the value of Nusselt number reaches a minimum.

This paper presents a numerical study of forced convection over a fluid/porous composite system. The system is composed of a relatively thin porous substrate attached to the surface of the flat plate. Since little is known about *external* forced convection fluid flow and heat transfer in the porous/fluid composite medium (to the best of authors' knowledge the present work constitutes the first analysis in this area), the present study is aimed at a fundamental investigation of the interaction phenomena occurring in the porous substrate and the fluid layer. The effects of various parameters governing the physics of the problem on the fluid flow and heat transfer are analyzed and the interfacial effects are systematically categorized. The accumulated knowledge gained through this investigation will provide a fundamental framework for predicting heat transfer and fluid flow characteristics for more complicated configurations.

2 Analysis

2.1 Mathematical Formulation. The coordinate system and the corresponding physical configuration are shown in Fig. 1. The thickness of the porous substrate is H, the free-stream velocity u_∞ and temperature T_∞ are constant, and the wall is maintained at constant temperature T_w. It is assumed that the flow is steady, laminar, incompressible, and two dimensional. In addition, the thermophysical properties of the fluid and the porous matrix are assumed to be constant and the fluid-saturated porous medium is considered homogeneous and isotropic and in local thermodynamic equilibrium with the fluid. The conservation equations for mass, momentum, and energy in the fluid region are

$$\nabla \cdot \mathbf{v} = 0 \tag{1}$$

$$\mathbf{v} \cdot \nabla \mathbf{v} = -\frac{1}{\rho_f} \nabla p + \nu_f \nabla^2 \mathbf{v} \tag{2}$$

$$\mathbf{v} \cdot \nabla T = \alpha_f \nabla^2 T \tag{3}$$

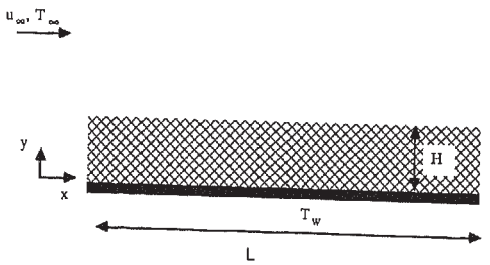

Fig. 1 Schematic of the coordinate system of the porous/fluid composite system

Contributed by the Heat Transfer Division for publication in the JOURNAL OF HEAT TRANSFER. Manuscript received by the Heat Transfer Division September 25, 1989; revision received February 27, 1990. Keywords: Augmentation and Enhancement, Forced Convection, Porous Media.

The conservation equations for the porous region are based on a general flow model, which includes the effects of flow inertia as well as friction caused by macroscopic shear (Vafai and Tien, 1981; Hong et al., 1985; Kaviany, 1987). This generalized flow model is also known as the Brinkman-Forchheimer-extended Darcy model. The governing equations for the porous layer are

$$\nabla \cdot \mathbf{v} = 0 \tag{4}$$

$$\mathbf{v} \cdot \nabla \mathbf{v} = -\frac{1}{\rho_f}\nabla p + \nu_{\text{eff}}\nabla^2 \mathbf{v} - \frac{\nu_f}{K}\mathbf{v} - \frac{F\delta}{\sqrt{K}}|\mathbf{v}|\mathbf{v} \tag{5}$$

$$\mathbf{v} \cdot \nabla T = \alpha_{\text{eff}}\nabla^2 T \tag{6}$$

where α_{eff} is defined as $\alpha_{\text{eff}} = k_{\text{eff}}/\delta\rho_f c_{p,f}$ and ρ_f and $c_{p,f}$ refer to the density and the heat capacity of fluid. It should be noted that the variables $\mathbf{v}$ and T are both volume-averaged quantities as described by Vafai and Tien (1981). The appropriate boundary conditions for the present problem are

$$u = u_\infty,\ v = 0,\quad p = p_\infty,\quad T = T_\infty,\ \text{at } x = 0 \tag{7}$$

$$u = 0,\quad v = 0,\quad T = T_w \qquad \text{at } y = 0 \tag{8}$$

$$u = u_\infty,\ p = p_\infty,\ T = T_\infty, \qquad \text{as } y \to \infty \tag{9}$$

In addition to these the following matching conditions have to be satisfied at the interface of the porous/fluid layer:

$$u|_{y=H^-} = u|_{y=H^+}, \qquad v|_{y=H^-} = v|_{y=H^+} \tag{10a}$$

$$p|_{y=H^-} = p|_{y=H^+}, \qquad \mu_{\text{eff}}\left.\frac{\partial v}{\partial y}\right|_{y=H^-} = \mu_f\left.\frac{\partial v}{\partial y}\right|_{y=H^+} \tag{10b}$$

$$\mu_{\text{eff}}\left(\frac{\partial u}{\partial y}+\frac{\partial v}{\partial x}\right)\Bigg|_{y=H^-} = \mu_f\left(\frac{\partial u}{\partial y}+\frac{\partial v}{\partial x}\right)\Bigg|_{y=H^+} \tag{10c}$$

$$T|_{y=H^-} = T|_{y=H^+}, \qquad k_{\text{eff}}\left.\frac{\partial T}{\partial y}\right|_{y=H^-} = k_f\left.\frac{\partial T}{\partial y}\right|_{y=H^+} \tag{10d}$$

These conditions express the continuity of longitudinal and transverse velocities, pressure, deviatoric normal and shear stresses, temperature, and the heat flux. The conditions expressed equation (10*b*) together imply matching of the total normal stress at the interface. The fifth condition in equation (10*c*) represents the matching condition for the shear stress, which is an extension of the condition used by Vafai and Thiyagaraja (1987) and Neale and Nader (1974) for flow that is not parallel to the porous/fluid interface. As rigorously proved by Vafai and Thiyagaraja (1987), matching of the stresses at the interfaces can only be accomplished if Brinkman's shear term is included in the momentum equation for the porous media.

It has been found that setting the effective viscosity of the fluid-saturated porous medium equal to the viscosity of the fluid provides good agreement with experimental data (Lundgren, 1972; Neale and Nader, 1974). This approximation is adopted in the present work. In addition the effect of thermal dispersion in the porous matrix is assumed to be constant and is incorporated in the effective thermal conductivity for simplicity in presentation of the results.

2.2 Numerical Simulations. Separate calculation schemes for the porous and fluid regions would require an involved iterative procedure for matching the interface conditions. A more efficient alternative is to combine the two sets of equations for the fluid region an the porous region into one set of conservation equations. In other words the porous substrate and the fluid region can be modeled as a single domain governed by one set of equations, the solution of which satisfies the continuity of the velocities, stresses, temperatures, and heat fluxes across the porous/fluid interface as described by equations (10*a-d*).

Introducing the stream function and the vorticity as

$$u = \frac{\partial \psi}{\partial y}, \qquad v = -\frac{\partial \psi}{\partial x}$$

$$\zeta = \frac{\partial v}{\partial x} - \frac{\partial u}{\partial y}$$

yields the dimensionless vorticity transport equation, stream function equation, and energy equation. These equations are valid throughout the composite layer.

$$\frac{\partial \psi^*}{\partial y^*}\frac{\partial \zeta^*}{\partial x^*} - \frac{\partial \psi^*}{\partial x^*}\frac{\partial \zeta^*}{\partial y^*} = \frac{1}{\text{Re}_L}\nabla^2\zeta^* + S^* \tag{11}$$

$$\nabla^2\psi^* = -\zeta^* \tag{12}$$

$$\frac{\partial \psi^*}{\partial y^*}\frac{\partial \theta}{\partial x^*} - \frac{\partial \psi^*}{\partial x^*}\frac{\partial \theta}{\partial y^*} = \nabla \cdot \left(\frac{1}{\text{Pe}_L}\nabla\theta\right) \tag{13}$$

where in the fluid region

$$\text{Re}_L = \frac{u_\infty L}{\nu_f}, \qquad \text{Pe}_L = \frac{u_\infty L}{\alpha_f}, \qquad S^* = 0 \tag{14a}$$

and in the porous region

$$\text{Pe}_L = \frac{u_\infty L}{\alpha_{\text{eff}}}, \qquad \text{Da}_L = \frac{K}{L^2}, \qquad \Lambda_L = \frac{FL\delta}{K^{1/2}} \tag{14b}$$

Nomenclature

C_f = friction coefficient, equation (17)
Da_L = Darcy number, equation (14*b*)
F = a function used in expressing inertia terms
h = convective heat transfer coefficient, $\text{Wm}^{-2}\text{K}^{-1}$
H = thickness of the porous medium, m
k = thermal conductivity, $\text{Wm}^{-1}\text{K}^{-1}$
K = permeability of the porous medium, m^2
L = length of the external boundary as shown in Fig. 1, m
Nu = Nusselt number, equation (18)
P = pressure, Pa
Pe_L = Peclet number, equation (14*a*) or (14*b*)
Pr = Prandtl number
Re_L = Reynolds number defined for the fluid region, equation (14)
T = temperature, K
u = x-component velocity, ms^{-1}
v = y-component velocity, ms^{-1}
$\mathbf{v}$ = velocity vector
x = horizontal coordinate, m
y = vertical coordinate, m
α = thermal diffusivity, m^2s^{-1}
α_{eff} = effective thermal diffusivity = $k_{\text{eff}}/\rho_f c_{p,f}$, m^2s^{-1}
δ = porosity of the porous medium
ζ = vorticity
Λ_L = inertia parameter, equation (14*b*)
μ = dynamic viscosity, $\text{kgm}^{-1}\text{s}^{-1}$
ν = kinematic viscosity, m^2s^{-1}
θ = dimensionless temperature
ρ = fluid density, kgm^{-3}
ψ = stream function

Subscripts

eff = effective
f = fluid
∞ = free stream

$$S^* = -\frac{1}{\mathrm{Re}_L \mathrm{Da}_L}\zeta^* - \Lambda_L |v^*|\zeta^* - \Lambda_L\left(v^*\frac{\partial|v^*|}{\partial x^*} - u^*\frac{\partial|v^*|}{\partial y^*}\right) \quad (15)$$

$$+\frac{u^*}{\mathrm{Re}_L}\frac{\partial}{\partial y}\left(\frac{1}{\mathrm{Da}_L}\right) - \frac{v^*}{\mathrm{Re}_L}\frac{\partial}{\partial x}\left(\frac{1}{\mathrm{Da}_L}\right)$$

$$+|v^*|u^*\frac{\partial}{\partial y}(\Lambda_L) - |v^*|v^*\frac{\partial}{\partial x}(\Lambda_L)$$

Note that all the variables have been nondimensionalized based on the following definitions:

$$x^* = \frac{x}{L}, \quad y^* = \frac{y}{L}, \quad u^* = \frac{u}{u_\infty}, \quad v^* = \frac{v}{u_\infty}$$

$$\psi^* = \frac{\psi}{u_\infty L}, \quad \zeta^* = \frac{L\zeta}{u_\infty}, \quad \theta = \frac{T - T_\infty}{T_w - T_\infty}$$

The dimensionless boundary conditions are

$$\psi^* = y^*, \quad \zeta^* = -\frac{\partial^2\psi^*}{\partial x^{*2}}, \quad \theta = 0 \quad \text{at } x^* = 0$$

$$\psi^* = 0, \quad \zeta^* = -\frac{\partial^2\psi^*}{\partial y^{*2}}, \quad \theta = 1 \quad \text{at } y^* = 0 \quad (16)$$

$$\frac{\partial\psi^*}{\partial y^*} = 1, \quad \zeta^* = -\frac{\partial^2\psi^*}{\partial x^{*2}}, \quad \theta = 0 \quad \text{as } y^* \to \infty$$

It is worthwhile to note that the boundary conditions at $x^* = 0$ and $y^* \to \infty$ are the same, i.e., the only difference is that at $x^* = 0$, ψ^* is specified and for $y^* \to \infty$, the gradient of ψ^*, i.e., $\partial\psi^*/\partial y^* = 1$, is specified. The downstream boundary conditions are discussed below. A control-volume-based finite difference method is employed to solve the system of elliptic partial differential equations for the vorticity, stream function, and temperature. The control volume formulation has the attractive feature that the resulting solution would imply that the integral conservation of mass, momentum, and energy is exactly satisfied over the whole domain as well as any group of control volumes. The physical domain was covered by a rectangular grid system consisting of m horizontal and n vertical lines. Extensive tests were carried out to determine the proper value of m and n for each numerical run. Each grid point was placed at the center of the corresponding control volume. A variable grid system was employed in the y direction, in the fluid region, in order to reduce the computational time. In this system, the grid spacing was based on a constant ratio between two adjacent increments (Anderson et al., 1984; Roache, 1972). The inlet boundary conditions were applied at a short distance upstream of the leading edge of the plate. It should be noted that as long as the inlet conditions are applied sufficiently upstream, it becomes immaterial where they are applied and the location of the inlet conditions will not affect the results. This procedure virtually eliminated the errors associated with the singular point at the leading edge of the composite system. In addition, the harmonic mean formulation suggested by Patankar (1980) was used to handle abrupt variations in thermophysical properties, such as the permeability and the thermal conductivity, across the interface. This ensured the continuity of the convective and diffusive fluxes across the interface without requiring the use of an excessively fine grid structure. Therefore, in the generalized formulation for the entire composite layer, to preserve all the interface boundary conditions, Λ_L and Da_L were treated as variables. However, in presenting the results the constant values of Λ_L and Da_L for the specified porous substrate that was analyzed were used.

In the present numerical scheme the space derivatives were approximated by a central-difference form except for the convective terms, which were approximated by using a second upwind-differencing scheme. It is worth mentioning that the source terms associated with the boundary and inertia effects were linearized according to a general recommendation by Patankar (1980). The finite difference equations thus obtained were solved by the extrapolated-Jacobi scheme. This iterative scheme is based on a double cyclic routine, which translates into a sweep of only half of the grid points at each iteration step (Adams and Oretega, 1982). It is noted that this scheme is vectorizable so that it can be used quite efficiently when used on a supercomputer. It was necessary to use underrelaxation to ensure convergence.

It was found that the downstream boundary conditions had quite a limited influence on the solution because the present problem had a significant parabolic character. Hence, the type of boundary condition specification on the right-hand side of the computational domain did not have much influence on the physical domain. Therefore, by using an extended computational domain, we were able to find very accurate results for our physical domain. That is, the computational domain was always chosen to be larger than the physical domain. We ran extensive tests on the effect of varying the size of the computational domain and observed its effects on the physical domain to ensure that the boundary conditions on the downstream side of the computational domain had no influence on our results. In our work, for simplicity, the conditions at the last interior grid points from the outflow boundary condition in the previous iteration were used and yielded the same solution for the domain of interest, except for the region very close to the downstream boundary as when the other conditions were used. For this reason the boundary conditions at the right-hand side of the domain were not explicitly given in equation (16).

Additional calculations were carried out in order to evaluate the effects of the porous material on the shear stress and heat transfer rate at the wall. The results for the shear stress were cast in dimensionless form by means of the local friction coefficient as

$$C_{f,x} = \frac{\tau_{w,x}}{\rho_f u_\infty^2/2} = \frac{2}{\mathrm{Re}_L}\frac{\partial u^*}{\partial y^*}\bigg|_{y^*=0} \quad (17)$$

and the results for the heat transfer rate were represented in dimensionless form in terms of a dimensionless Nusselt number

$$\mathrm{Nu}_x = \frac{hx}{k_f} = -x^*\frac{k_e}{k_f}\frac{\partial\theta}{\partial y^*}\bigg|_{y^*=0} \quad (18)$$

It should be noted that the conductivity of the fluid was chosen in the formation of the Nusselt number. This choice resulted in more meaningful comparisons for the heat flux at the external boundary between the composite system and the case where there was no porous substrate.

2.3 Stability and Accuracy of the Numerical Scheme. The numerical integration was performed until the following convergence criterion was satisfied:

$$\max\left|\frac{\varphi_{i,j}^{n+1} - \varphi_{i,j}^n}{\varphi_{i,j}^n}\right| < 10^{-6} \quad (19)$$

where φ stands for ζ^*, ψ^*, or θ and n denotes the iteration number. The stability of the numerical scheme was found to be somewhat insensitive to the choice of Δx and Δy. We employed a proper combination of Δx and Δy to assure stability. This was done by a systematic decrease in the grid size until further refinement of the grid size showed no more than a 1 percent difference in the convergent results.

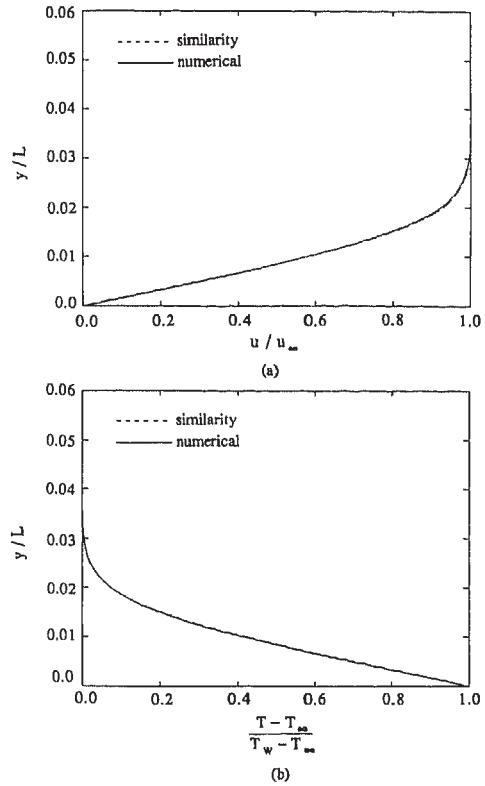

Fig. 2 Comparison of numerical solutions with the similarity solutions for convective flow over a semi-infinite flat plate: (*a*) velocity distribution, (*b*) temperature distribution

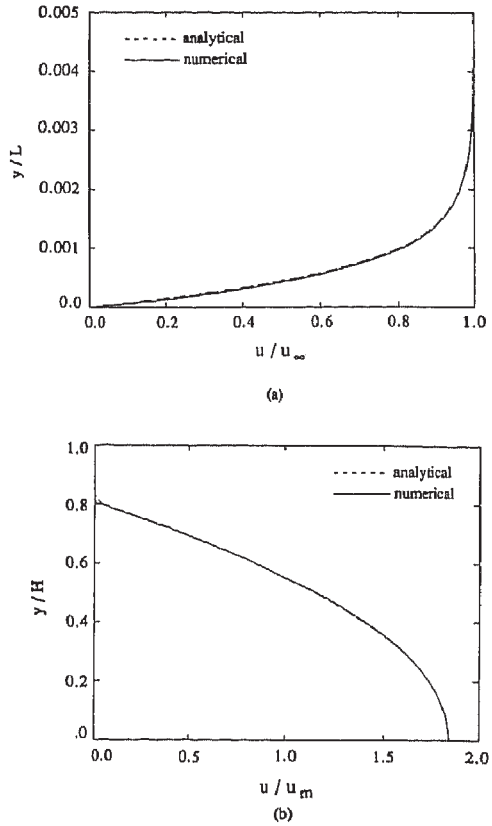

Fig. 3 Comparison of numerical solutions for the velocity with the corresponding analytical solutions: (*a*) flow over a flat plate embedded in a porous medium, (*b*) flow in a channel partially filled with a porous medium

The application of the boundary condition at infinity at a finite distance from the wall was given careful consideration. This was done through the following procedure. The length of the computational domain in the vertical direction was systematically increased until the maximum vorticity changes for two consecutive runs became less than 1 percent. Comparisons with more classical results were made in order to validate the present numerical model. The results for $H^* = 0$ (no porous substrate) agree to better than 1 percent with boundary layer similarity solutions for velocity and temperature fields as shown in Figs. 2(*a*) and 2(*b*). In these figures the Reynolds number based on the characteristic length was 3×10^5 and the Prandtl number of the fluid was taken to be 1.0. Note that this limiting case simply corresponds to forced convection over a flat plate. Also the results for $H^* \to \infty$ (full porous medium) agree to better than 1 percent with boundary layer analytical solutions by Vafai and Thiyagaraja (1987) and Beckerman et al. (1987). The results of such a comparison for a case where the product of the Reynolds number, Darcy number, and the inertia parameter was 1.0 are shown in Fig. 3(*a*). Note that this limiting case corresponds to flow over a flat plate embedded in a porous medium.

In addition to these two limiting cases, the numerical solutions for the velocity field in a porous/fluid composite medium using the present numerical code were compared with the analytical solution by Poulikakos and Kazmierczak (1987) for the problem of hydrodynamically and thermally fully developed forced convection in a channel partially filled with a porous medium. The results of this comparison for a case where the thickness ratio of the porous material to channel width is 0.2 and the Darcy number based on the channel width is 10^{-4} are presented in Fig. 3(*b*). As a final check, the problem of fully developed flow over a porous/fluid composite layer was solved using the present numerical code and compared with the analytical solution presented by Vafai and Thiyagaraja (1987). It was found that there is a very good agreement between the analytical and numerical results. Through the above-mentioned series of tests it was confirmed that the numerical model used in the present work predicts quite accurately the velocity and temperature fields in a porous/fluid composite system.

3 Results and Discussion

The effects of the porous substrate on the velocity and temperature fields are illustrated in Fig. 4 for a case where the Darcy number is 8×10^{-6}, the inertia parameter is 0.35, and the dimensionless thickness of the porous substrate is 0.02. Also shown in these figures are the velocity and temperature profiles for the case where no porous substrate is present. It should be noted that the effects of the porosity variation and the thermal dispersion in the porous region can change the results because of the channeling effect and the dynamic heat transfer mechanism (Vafai, 1986). However, the main features presented in this work will prevail even for the case where variable porosity effects are important. It can be seen that two distinct momentum boundary layers exist: one in the porous region and the other in the fluid region. Inside the porous region the velocity profile is shown to increase from zero to a certain constant value as the transverse coordinate increases. This constant value is maintained until the outer boundary layer appears. This velocity profile then goes through a smooth transition across the porous/fluid interface and approaches a free-stream value in the fluid region. As expected, the momentum boundary layers in the porous substrate as well as the fluid region grow as the streamwise coordinate increases. As a result the magnitude of the interfacial velocity decreases to accommodate this growth. Physically this is the result of a continuous displacement of fluid (or blowing) from the porous region into the fluid region due to the relatively larger resistance that the flow experiences in the porous region. This blowing

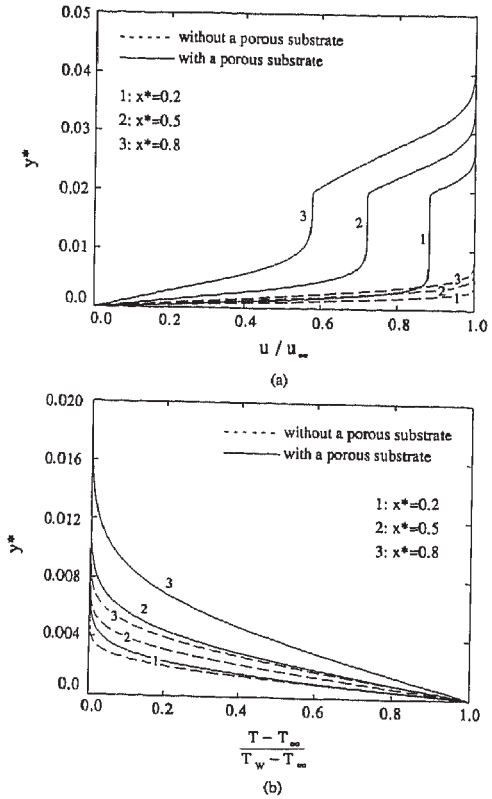

Fig. 4 (*a*) **Velocity and** (*b*) **temperature distribution along the flat plate at three different locations,** $x=0.2$, 0.5, **and** 0.8, **for** $Da_L = 8\times10^{-6}$, $\Lambda_L = 0.35$, $k_e/k_f = 1.0$, $H^* = 0.02$

effect becomes less pronounced as the amount of flow into the porous region becomes smaller. It can be seen from Fig. 4(*a*) that the attachment of the porous substrate onto the flat plate results in a significant decrease in the frictional drag at the wall. This decrease is a direct result of the blowing effect previously discussed. It should be noted that the frictional resistance at the porous/fluid interface is essentially negligible. However, this condition of negligible frictional drag at the porous/fluid interface was not imposed in our solution scheme, it was a fact that was the outcome of our numerical results. The matching of the shear stress, equation (10*c*), will then ensure that the frictional resistance on both the fluid side and the porous side at the porous/fluid interface is negligible. This can be observed upon careful examination of Fig. 4(*a*) around the narrow interface region.

The temperature field shown in Fig. 4(*b*) corresponds to a case where the Prandtl number is 0.7 and the conductivity of the porous medium is equal to that of the fluid. It can be seen that the heat transfer rate at the wall is lower for the case in which a porous substrate is attached to the external boundary. This is due to lower velocities at the wall, which in turn diminish the convective energy transport for the case where the porous substrate is present. It is this decrease in the transport of the convective energy that causes a lower temperature gradient and heat flux at the wall for the composite system. The influence of Reynolds number comes through changes in the slopes of the curves shown in Fig. 4. However, the main feature of the results presented in Fig. 4 will also prevail for different Reynolds numbers, i.e., a decrease in the frictional drag and the heat transfer at the wall for the case where the porous substrate is attached to the wall. It should be noted that the thickness of the thermal boundary layer depends on the Prandtl number and the ratio of the conductivity of the porous material to that of the fluid. Therefore, the porous substrate could be designed such that it would either enhance or retard the transfer of energy to the impermeable boundary.

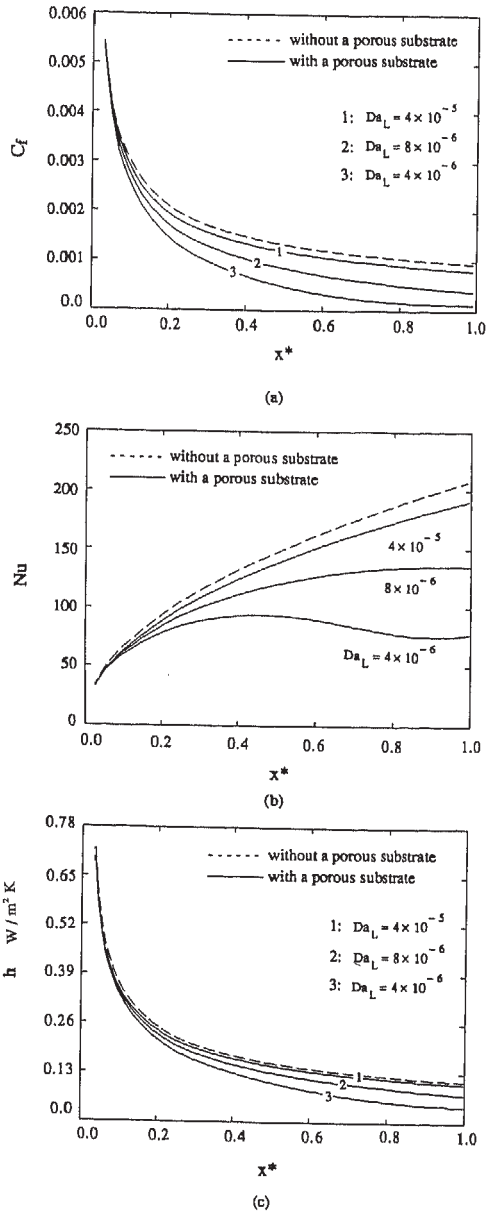

Fig. 5 Effects of the Darcy number on (*a*) **friction coefficient,** (*b*) **Nusselt number, and** (*c*) **convection heat transfer coefficient variation along the flat plate for** $\Lambda_L = 0.0$, $Pr = 0.7$, $k_e/k_f = 1.0$, $H^* = 0.02$

Effect of the Darcy Number. The Darcy number, as can be seen from equation (14*b*), is directly related to the permeability of the porous medium. Figure 5 shows the streamwise variations of the local friction coefficient and the Nusselt number, C_f and Nu, for various Darcy numbers. In order to concentrate only on the effects of the Darcy number the inertial effects were neglected in obtaining the results displayed in Fig. 5. As expected the local friction coefficient at the wall decreases as the Darcy number decreases. This is because smaller values of Da relate to larger bulk frictional resistance to the flow in the porous substrate. This in turn causes a lower velocity gradient at the wall. Also, as expected, the frictional drag at the wall approaches that of the case without the porous substrate for larger values of the Darcy number. As shown in Fig. 5(*b*), the Nusselt number values for the case with a porous substrate are lower than the case where no porous substrate is present. This is because the presence of the porous substrate and/or smaller value of Da translate into smaller velocities near the impermeable boundary, which in turn diminish the transfer of the convective energy. The peculiar variation in the Nusselt

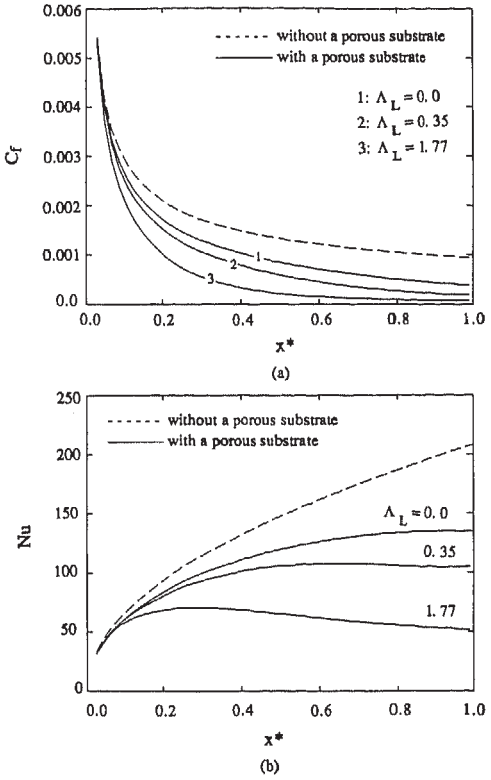

Fig. 6 Effects of the inertia parameter on the friction coefficient and the Nusselt number for $Da_L = 8 \times 10^{-6}$, Pr = 0.7, $k_e/k_f = 1.0$, $H^* = 0.02$

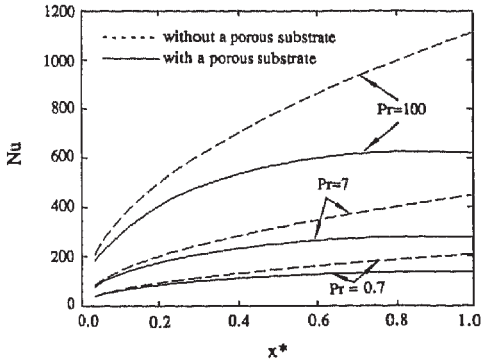

Fig. 7 Effects of the Prandtl number on the Nusselt number for $Da_L = 8 \times 10^{-6}$, $\Lambda_L = 0.0$, $k_e/k_f = 1.0$, $H^* = 0.02$

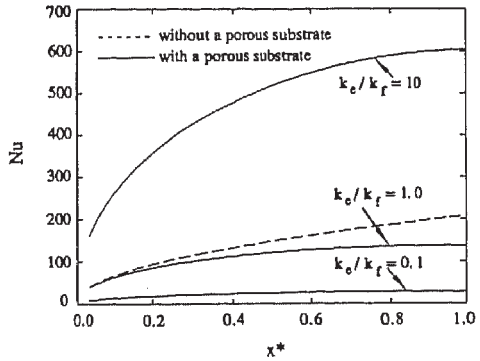

Fig. 8 Effects of the ratio of the conductivity of the porous medium to that of the fluid on the Nusselt number for $Da_L = 8 \times 10^{-6}$, $\Lambda_L = 0.0$, Pr = 0.7, $H^* = 0.02$

number distribution for smaller values of Darcy numbers is directly related to the way the Nusselt number is defined. First, it should be noted that the Nusselt number is linearly proportional to the product of the heat transfer coefficient, h, and the axial distance x. However, the heat transfer coefficient itself is also a function of x. Specifically h is a decreasing function of x. As can be clearly seen in Fig. 5(c), the rate of decrease of the heat transfer coefficient changes significantly over the length of the plate. It is exactly this nonuniform rate of decrease in h that causes the type of variation in the Nusselt number shown in Fig. 5(b). Therefore as the curvature of the heat transfer coefficient h changes at different axial locations, then depending on the rate of decrease of h at a particular axial location versus the rate of increase of the linear function x, we can get either an increasing or decreasing Nusselt number at that particular location.

Inertial Effects. As pointed out by a number of previous investigators, the inertial effects become significant when the Reynolds number based on the pore diameter becomes large. The effect of the inertial parameter is depicted in Fig. 6 for a fixed value of the Darcy number, $Da_L = 8 \times 10^{-6}$. The larger the inertial parameter, the larger will be the bulk frictional resistance that the flow will experience. Consequently the mass flow rate through the porous substrate decreases. Therefore larger value of Λ_L would result in a larger blowing effect through the porous substrate, which would consequently create thicker boundary layer thicknesses as well as a reduction in the friction coefficient and the Nusselt number values. The computed results confirm these facts and reveal that the thickness of the boundary layer increases as the inertial parameter increases. Also as expected the friction coefficient and the Nusselt number values decrease as the inertial parameter increases.

Prandtl Number Effects. The Prandtl number effects are shown in Fig. 7 for a fixed value of the Darcy number, $Da_L = 8 \times 10^{-6}$ and $\Lambda_L = = 0$. In this figure, the Nusselt number variation along the streamwise coordinate are shown for three different Prandtl numbers for two different cases. These cases refer to situations where the porous substrate is present and where it is absent. The values for the Prandtl number—0.7, 7.0, and 100—are such that they will cover a wide range of thermophysical fluid properties. So, for example, fluids such as air, water, and several different oils are well represented by the chosen values. As expected, the Nusselt numbers for both cases increase with an increase in the Prandtl number. However, there is a significant difference between the values of the Nusselt number for the two cases. The reasons for these differences were given previously when the effects of the Darcy number were discussed.

Effects of the Conductivity Ratio. The effect of the thermal conductivity ratio is shown in Fig. 8 for a fixed value of the Darcy number, $Da_L = 8 \times 10^{-6}$ and $\Lambda_L = 0$. As expected an increase in the conductivity ratio, k_e/k_f, where k_e is the effective conductivity of the porous medium and k_f is that of the fluid, results in an increase in the Nusselt number. It is important to note that the heat transfer rate at the wall for the case where a porous substrate is attached can be either greater or less than the case where no porous substrate has been used. The determining parameter as to whether the heat transfer will increase or decrease with the attachment of the porous substrate is the conductivity ratio, k_e/k_f. Therefore both the heat transfer enhancement or retardation of an external boundary can be achieved through the attachment of a porous substrate.

4 Conclusions

Forced convection over an external boundary lined with a porous substrate has been investigated in the present work. The characteristics of the velocity and temperature fields have been researched. Consideration was given to convective flows that exhibit boundary layer characteristics. However, the boundary layer approximation was not used. Comparisons of the friction coefficient and the Nusselt number between the

composite system and the case where no porous substrate was used revealed a number of physically interesting phenomena. Two distinct boundary layers were shown to exist for the velocity field while only one boundary layer was observed for the temperature field. It was shown that the porous substrate significantly reduces the frictional drag and the heat transfer rate at the wall. Therefore this configuration can be used as a frictional drag reducer for flows that have a parabolic character. It should be noted that here we are referring to the frictional drag and not the total drag. A momentum balance on a control volume extending from the plate surface out into the free stream, and accounting for pressure forces across the control volume, would provide us with the magnitude of the total drag. It has been shown that both heat transfer retardation and enhancement of an external boundary can be achieved through the attachment of a porous substrate. Furthermore, the effects of the governing parameters such as the Darcy number, inertia parameter, Prandtl number, and conductivity ratio of the porous material to the fluid were also investigated.

References

Adams, J., and Ortega, J., 1982, "A Multicolor SOR Method for Parallel Computation," *Proceedings of Int. Conf. on Parallel Processing*, pp. 53-56.

Anderson, D. A., Tannehill, J. C., and Pletcher, R. H., 1984, 1984, *Computational Fluid Mechanics and Heat Transfer*, Hemisphere Publishing Corp., New York.

Beckermann, C., Ramadhyani, S., and Viskanta, R., 1987, "Natural Convection Flow and Heat Transfer Between a Fluid Layer and a Porous Layer Inside a Rectangular Enclosure," ASME JOURNAL OF HEAT TRANSFER, Vol. 109, pp. 363-370.

Beckermann, C., Viskanta, R., and Ramadhyani, S., 1988, "Natural Convection in Vertical Enclosures Containing Simultaneously Fluid and Porous Layers," *J. Fluid Mechanics*, Vol. 186, pp. 257-284.

Hong, J. T., Tien, C. L., and Kaviany, M., 1985, "Non-Darcian Effects on Vertical-Plate Natural Convection in Porous Media With High Porosities," *Int. J. Heat Mass Transfer*, Vol. 28, pp. 2149-2157.

Kaviany, M., 1987, "Boundary-Layer Treatment of Forced Convection Heat Transfer From a Semi-infinite Flat Plate Embedded in Porous Media," ASME JOURNAL OF HEAT TRANSFER, Vol. 109, pp. 345-349.

Lundgren, T. S., 1972, "Slow Flow Through Stationary Random Beds and Suspensions of Spheres," *J. Fluid Mechanics*, Vol. 51, pp. 273-299.

Neale, G., and Nader, W., 1974, "Practical Significance of Brinkman's Extension of Darcy's Law: Coupled Parallel Flows Within a Channel and a Bounding Porous Medium," *Canadian Journal of Chemical Engineering*, Vol. 52, pp. 475-478.

Patankar, S. V., 1980, *Numerical Heat Transfer and Fluid Flow*, Hemisphere Publishing Corp., New York.

Poulikakos, D., 1986, "Buoyancy-Driven Convection in a Horizontal Fluid Layer Extending Over a Porous Substrate," *Phys. Fluids*, Vol. 29, pp. 3949-3957.

Poulikakos, D., and Kazmierczak, M., 1987, "Forced Convection in a Duct Partially Filled With a Porous Material," ASME JOURNAL OF HEAT TRANSFER, Vol. 109, pp. 653-662.

Roache, P. J., 1972, *Computational Fluid Dynamics*, Hermosa, Albuquerque, NM.

Sathe, S. B., Lin, W. Q., and Tong, T. W., 1988, "Natural Convection in Enclosures Containing an Insulation With a Permeable Fluid-Porous Interface," *Int. J. Heat Fluid Flow*, Vol. 9, pp. 389-395.

Vafai, K., 1986, "Analysis of the Channeling Effect in Variable Porosity Media," ASME *Journal of Energy Resources Technology*, Vol. 108, pp. 131-139.

Vafai, K., and Thiyagaraja, R., 1987, "Analysis of Flow and Heat Transfer at the Interface Region of a Porous Medium," *Int. J. Heat Mass Transfer*, Vol. 30, pp. 1391-1405.

Vafai, K., and Tien, C. L., 1981, "Boundary and Inertia Effects on Flow and Heat Transfer in Porous Media," *Int. J. Heat Mass Transfer*, Vol. 24, pp. 195-203.